Ti6Al4V Hybrid Structure Mechanical Properties – Wrought and Additive Manufactured Powder-Bed Material

O. Dolev*, S. Osovski and A. Shirizly

Faculty of Mechanical Engineering, Technion, Haifa 3200003, Israel

* dolev.ohad@gmail.com

Abstract

The implementation of additive manufacturing techniques in the production of mission critical structural components is challenged by its low throughput and limited build envelope. In recent years, hybrid production methods are emerging to bridge between the build volume and high throughput of conventional production methods and the design freedom enabled by additive manufacturing. The repeatability of material properties and the quality of the interface between the additive manufactured and wrought material are crucial for the adoption of hybrid manufacturing techniques by the industry. Here, the tensile behavior and fracture toughness of a hybrid Ti6Al4V alloy are examined in detail. Ti6Al4V pre-forms were built onto a wrought Ti6Al4V start-plate and extracted via milling. Compact tension and uniaxial tension specimens, extracted from the hybrid pre-forms demonstrated good fracture and properties with no preference for crack growth in neither the AM or wrought materials. Microstructural characterization revealed a sharp interface between the two materials with no evidence of a heat-affected zone. The hybrid manufacturing approach studied here expands the current limitations of large scale critical components with fine features and allow such structures to be produced with a higher thruput.

Keywords: Additive manufacturing, Hybrid manufacturing, Fracture-toughness, Powder bed

1. Introduction

Titanium and its alloys pose a unique combination of physical and mechanical properties such as high specific strength, high toughness, good corrosion resistance [1–6], etc. As such, Titanium alloys are often found in damage-critical load-bearing structures and weight critical products. Among the various Titanium alloys, Ti-6Al-4V stands out as being one of the most frequently used Titanium alloys in the industry. It is not a surprise then, that with the emergence of additive manufacturing (AM) techniques, Ti-6Al-4V was one of the first metallic material to be incorporated into a commercial critical component [7]. Throughout the development of AM technology, Ti-6Al-4V was studied extensively in the scientific literature [8–17] as well as by aerospace and BioMed industries. Over the last decade, Ti-6Al-4V was intensively integrated into various additive manufacturing processes, demonstrating remarkable business case reasoning through improved functionality, efficient material usage, and cost reduction.

Powder bed additive manufacturing is considered to be a low throughput manufacturing method, with a limited build envelope, thus landing itself mostly for the production of high-quality structures with fine features, very thin walls, lattice structures, fine internal channels, and cavities. In recent years, Hybrid AM - conventional manufacturing processes are emerging as a viable way to overcome the build limitations of AM, thus enhancing the functionally and expanding reach of the AM technology [18,19]. Hybrid manufacturing processes pose a significant technological advance, allowing for component repairs [20–23], production of bi-materials [24–28], and manufacturing of large components with intricate designs [25,29–32]. Hybrid manufacturing techniques, consisting of both powder bed fusion and wire arc AM hold a promise to result in a manufacturing method which marks the benefits of both worlds, i.e. relative freedom of design along with rapid manufacturing process [33]

With the growing interest in AM of metallic components, the mechanical properties resulting from various powder bed and direct energy deposition techniques have been extensively studied in the literature. As can be observed from [34,35] and references within, both the static (e.g. tensile strength, elongation to failure, etc.) properties, as well as mechanical anisotropy, fracture toughness, and fatigue life, are highly dependent on the process parameters and has been studied extensively. However, for Hybrid manufactured components, the majority of works cited above, have focused on the microstructural characterization and uniaxial tension behavior solely (e.g. [33,36]). Only a few works have studied the fracture properties of Hybrid structures [11,37].

The work presented here is aimed at characterizing the fracture toughness of a Hybrid Ti-6Al-4V structure, produced via selective laser melting (SLM) and subtractive manufacturing of the base plate (wrought Ti-6Al-4V) on which it was manufactured. The rest of the paper is organized as follows: We first describe the experimental procedure by which the hybrid structure was fabricated along with a description of the experimental approach. Next, the microstructure surrounding the AM-Wrought interface is presented along with the measured hardens variations. The uniaxial mechanical behavior and fracture toughness of the Hybrid material is then compared to those of the wrought and AM material, demonstrating the feasibility of the

proposed manufacturing route for load-bearing, damage critical components. The main findings of the work are then briefly summarized.

2. Experimental

2.1 Specimens fabrication

An EOS M280 powder bed SLM was used to build a series of pre-forms designated for tensile tests (round rods) and fracture toughness evaluation (cubes). The pre-forms were fabricated from a 30-microns Ti-6Al-4V powder supplied by TLS Technik GmbH. Both the powder and build plate were used in their virgin form i.e. have not experienced any prior heat cycle. The process parameters are given in Table 1. The substrate material for the hybrid specimens manufacturing was wrought chosen to be Ti-6Al-4V cold-rolled plate purchased from TITANIUM INTERNATIONAL GROUP SRL. No support structures were used in the building process to facilitate the mechanical evaluation of the hybrid material. The various pre-forms used for this study and their designation are given in Figure 1 along with an illustration of the tensile and compact-tension fracture specimens overlaid on the pre-forms.

Table1: SLM process parameters

Power	Scan speed	Hatch distance	Hatching strategy
175W	1250 mm/sec	0.012mm	Line

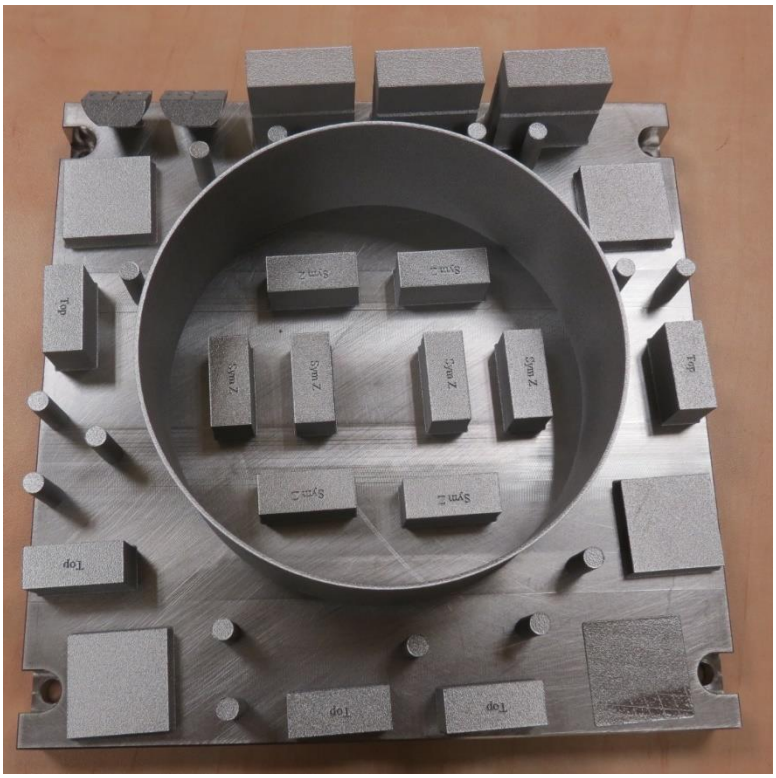

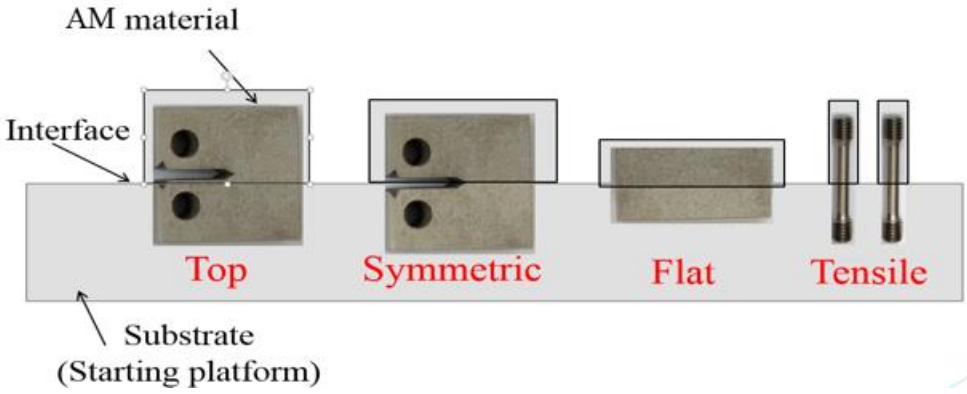

Figure 1: Built pre-forms (AM) on the wrought Ti-6Al-4V substrate plate (top) and an illustration of the pre-forms overlaid with the specimens before post-processing (bottom).

Following the SLM process pre-forms were carefully machined out of the substrate plate and AM material. The pre-forms from the three groups (i.e. hybrid, AM and wrought) were heat-treated following two commonly used procedures for AM Ti-6Al-4V, namely: 650°C for 3h or 800°C for 4h. Both heat treatments were held and cooled in vacuumed furnace. Finally, the pre-forms were machined into tensile specimens (Figure 2a, in accordance with ASTM E8) and compact-tension (CT) specimen (Figure 2b, following ASTM E399-17). The tensile specimens' geometry was selected to comply with the geometrical limitations induced by the plate thickness. Special care was taken while machining the specimens to ensure that the AM-wrought interface is located at:

i. The center of the gauge for the tensile specimens.
ii. Bellow the notch tip and parallel to the CT specimen's symmetry plane (designated as "Top")
iii. Directly ahead of the notch tip and along the CT specimen's symmetry plane (designates "Symmetric").
iv. Halfway through-thickness of the CT specimen, perpendicular to the crack growth direction (designated "Flat")

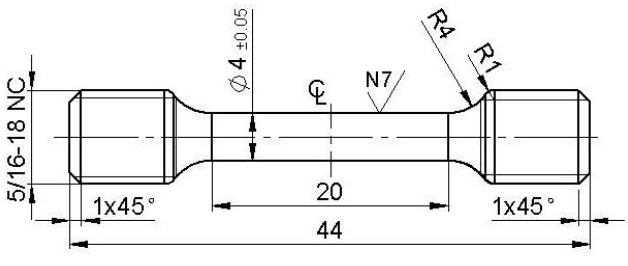

(a)

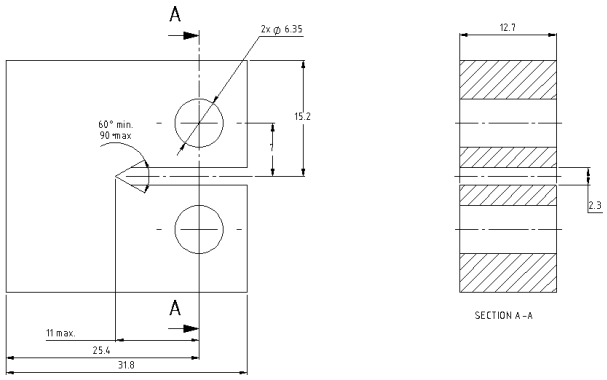

(b)

Figure 2: (a) ASTM E8 tensile specimen's geometry and dimensions. (B) ASTM E399-17 CT specimen's geometry and dimensions.

In addition to the Hybrid specimens, tensile and CT specimens were machined out of purely AM material (manufactured via the same preforms and on the same plate in the same batch) as well as from the wrought plate serving as substrate. The tensile specimens extracted from the substrate plate (i.e. wrought material). We acknowledge that the tensile test results reported for the wrought material may be different in the rolling direction when compared to the through-thickness direction used for the hybrid specimens. However, through-thickness tensile specimens, complying with the dimensions of ASTM E8 could not be extracted due to the plate thickness.

2.2 Microstructural observations

Hybrid samples were extracted and then ground and polished using SiC (1000#) followed by colloidal silica (0.04 microns). The polished specimens were lightly etched by swabbing with Kroll's reagent to expose the underlying microstructure. An Olympus BX-51 optical microscope and a high-resolution TESCAN MIRA-3 FEG-SEM were used to study the microstructure surrounding the interface.

Nondestructive testing using Micro-focus Computerized scanner Testing (Nikon XT H 320 CT Scanning system with a 225 kV micro-focus source, equipped with a reflection target, allowing a 3-micron spot size), was used to assess the porosity levels as discussed in Section 3.

2.3 Mechanical testing

Vickers micro-hardness testing was done using Shimadzu HMV-G20 operating at a load of 500gfr.

The tensile tests were carried out using a 100KN Instron tensile machine at a strain rate of $7x10^{-3}$ s^{-1}. Displacement in the AM and wrought tensile experiments were measured using a 25 mm mechanical extensometer (Instron). For the Hybrid tensile tests, prior to conducting the experiments, a black and white speckle pattern was applied via an airbrush and imaged to extract the displacements along the specimen's gage using GOM-ARAMIS digital image correlation (DIC) software.

The compact tension specimens were first fatigue pre-cracked using an Instron 8801 testing machine (Dynacell, Dynamic Load Cell +/- 100 kN) under load control with a sinusoidal waveform in the air at 22±3°C @ 15 Hz. The cyclic loading of the fatigue pre cracking was applied with a load ratio of R=0.1 and a maximum load of 3 kN (200-500K cycles). The maximum stress intensity in the terminal (2.5 %) stage of fatigue crack growth did not exceed 80 % of the KIC value. The crack propagation was monitored using a crack opening displacement gage (COD gage) and visually monitoring the crack growth on the sides of the specimens.

3. Results and discussion

3.1 Microstructural observations

In Figure 3., SEM images of the AM-wrought interface, taken at three magnifications (view fields of 20μm,120μm, and 750μm) are presented for a hybrid specimen heat treated at 800°C for 4 hours. No porosity or other discontinuities were observed along the AM-wrought interface, which in turn seemed to be very sharp even at larger magnifications (not presented in the paper).

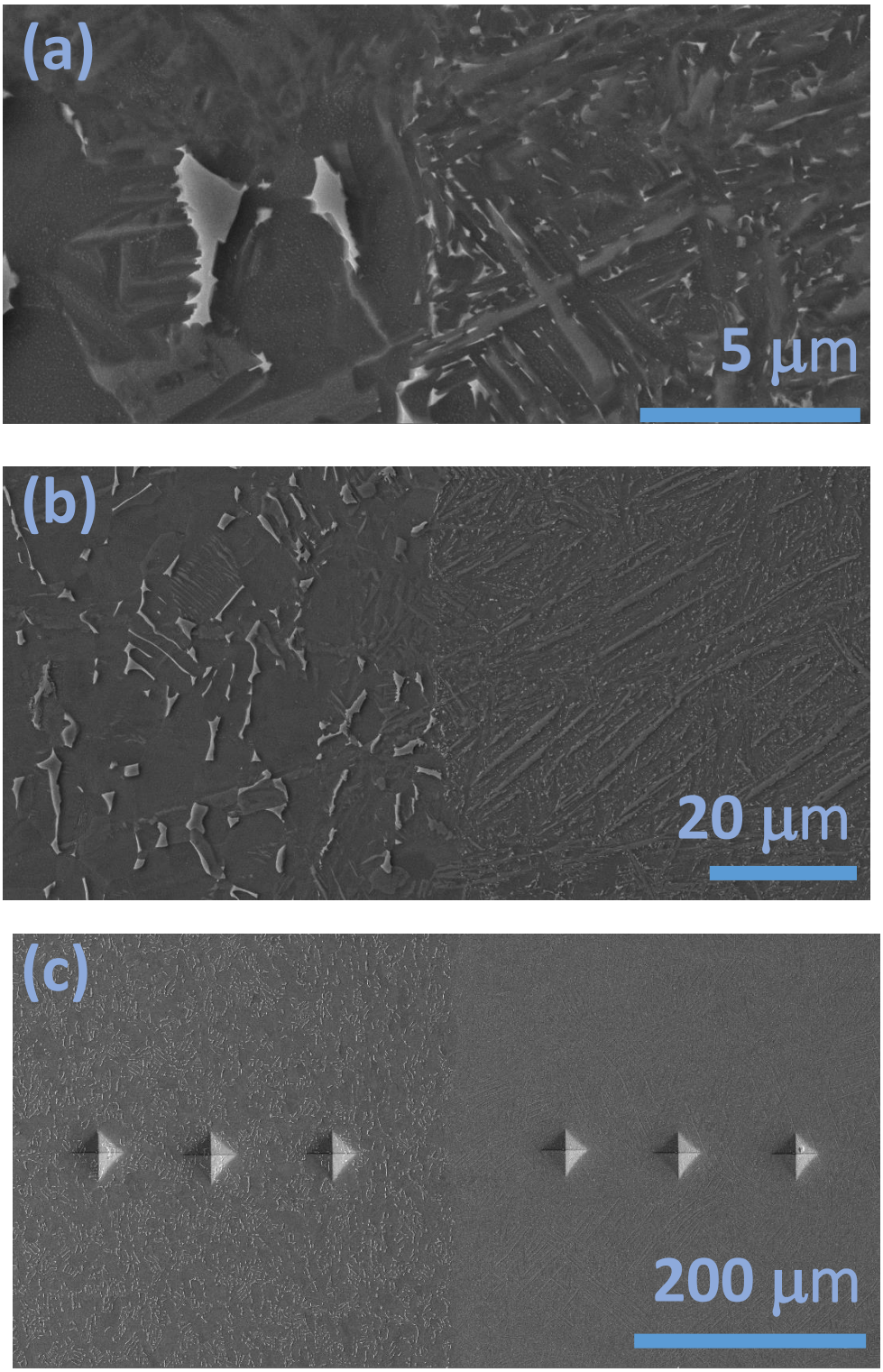

Figure 3: Secondary electron images were taken at the interface of a hybrid specimen heat treated at 800oC for 4hours (AM is on the right side). (a) 20mm view field (x27.7K). (b) 120mm view field (x4.6k). (c) 750mm (x740k). Notice the absence of defects or a heat-affected zone.

Since the SLM process can be considered as a welding type of manufacturing, in which the powder beads are being welded together, one might expect the resulting microstructure at the AM-wrought interface to be similar to those observed after laser beam welding (LBW) of AM Ti-6Al-4V to its wrought counterpart (e.g. [38]). Surprisingly, no heat-affected zone was observed and the microstructure remained consistent in appearance for both the AM and wrought sides even at distances of more than 1mm away from the interface. Optical microscopy was employed to demonstrate the absence of HAZ and apparent uniformity in microstructure away from the AM-wrought interface. As is evident from Figure 4, no HAZ is observed even for lower magnifications.

Figure 4: Optical microscopy image of the AM (left)-wrought (right) interface taken at a magnification of 5X

Micro-hardness tests (HV) taken at equal distances from the interface (Figure 5), from both wrought and AM regions, indicate a slight decrease in hardness at a distance of up to 100μm away from the interface for the wrought material and 200μm for the AM material, which quickly regains back to typical values of ~318HV material and 350HV for the AM material. Note however that both materials exhibit a second small drop in hardness at ~900 μm away from the interface.

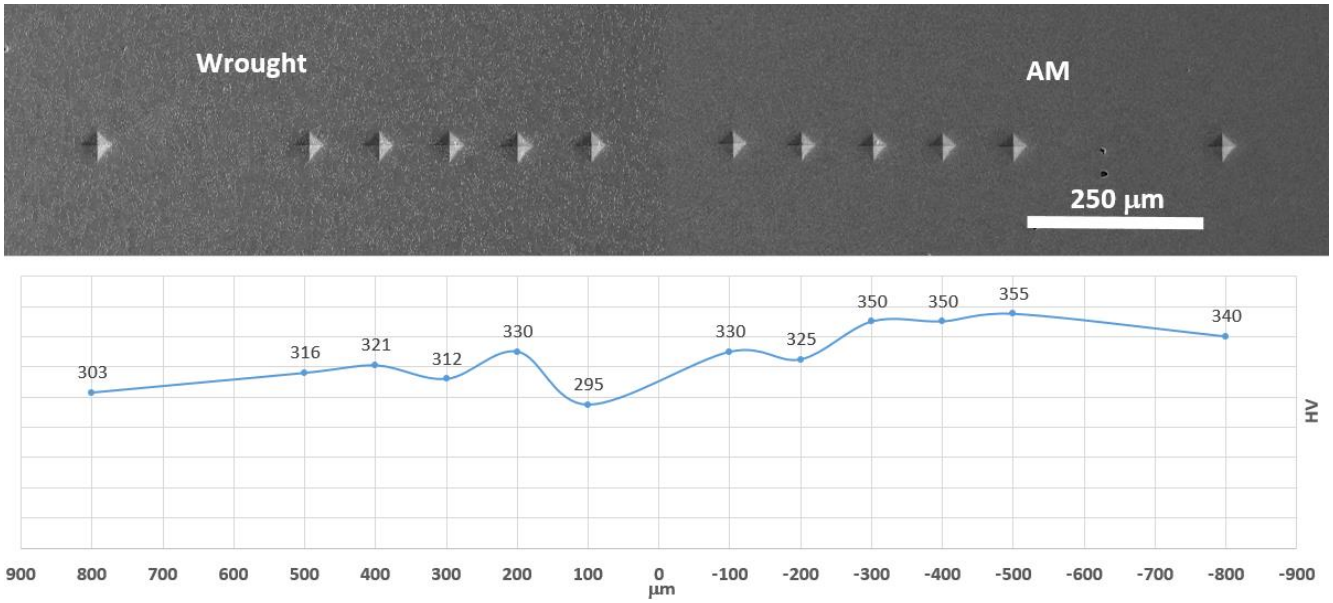

Figure 5: Micro-hardness profile along the longitudinal direction of the hybrid sample as a function of distance from the interface.

Unfortunately, we were not able to correlate the lower hardness values with any apparent microstructural variations with the instrumentation at hand. At this stage we attribute the absence of a HAZ to the thermal cycles experienced by the material throughout the SLM process, however, this has to be further studied to obtain a definite answer.

3.2 Uniaxial tensile tests

All three groups of tensile specimens (i.e. AM; wrought; hybrid) were tested under uniaxial tension. Two series of measurements were conducted for the AM and wrought groups of specimens, each corresponding to one of the heat treatments described above (i.e. 800°C for 4h and 650°C for 3h). The number of (successful) tests performed for each condition is summarized in Table 2 along with the average measured properties and standard errors.

Table 2: Summary of tensile tests

Sample description	Number of samples	Yield stress [MPa]		Ultimate Tensile Strength [MPa]		Elongation [%]		Reduction of Area [%]	
SLM; HT - 650°C ; 3h	7	1093	±15.3	1174	±10.2	8.7	±2.3	29	±8.2
SLM; HT - 800°C ; 4h	10	904	±8.3	997	±7.9	15.8	±2.7	48.7	±1.8
Wrought; HT - 650°C ; 3h	5	860	±23.5	943	±29.8	14.1	±1.2	33.2	±7.1
Wrought; HT - 800°C ; 4h	5	839	±18.9	928	±14.7	14	±1.2	34.6	±12.2
Hybrid; HT - 800°C ; 4h	9	845	±14.6	937	±9.8	11.9	±1.3	31.8	±6.9

As evident from Figure 6, increasing the temperature of the heat treatment from 650°C to 800°C has a very limited effect on the measured properties of the wrought material. On the other hand, the AM material which underwent a heat treatment of 800°C for 4 hours exhibited a ~10% decrease in yield and ultimate tensile stress while almost doubling the elongation to failure and reduction of area. For both heat treatments, the AM material is found to be stronger when compared to the wrought, albeit being less ductile when undergoing the 650°C /3 hours heat treatment.

Following the tensile tests of the wrought and AM materials, it was decided to subject the Hybrid material to the 800°C/4hours treatment for all measurements to come. The tensile tests, conducted on the hybrid material, have demonstrated a yield and ultimate stress values similar to the ones obtained for the wrought material undergoing the same heat treatment. Similarly, the measured reduction of area was found to be the same in the wrought and hybrid specimens' groups. In contrast to the aforementioned material parameters, the elongation to failure was found to be slightly lower in the hybrid material (11.9 ± 1.3 compared to 13 ± 1.2). This close similarity in mechanical properties raises a question as to the role played by the AM side of the hybrid tensile specimen. Moreover, it was observed that in all of the 9 hybrid specimens, necking and failure were observed solely on the wrought side. This observation is illustrated in Figure 7, where two failed hybrid specimens are presented after being ground, polished and etched to expose the microstructure and hence aid in identifying which side belongs to which material as well as the location of the interface.

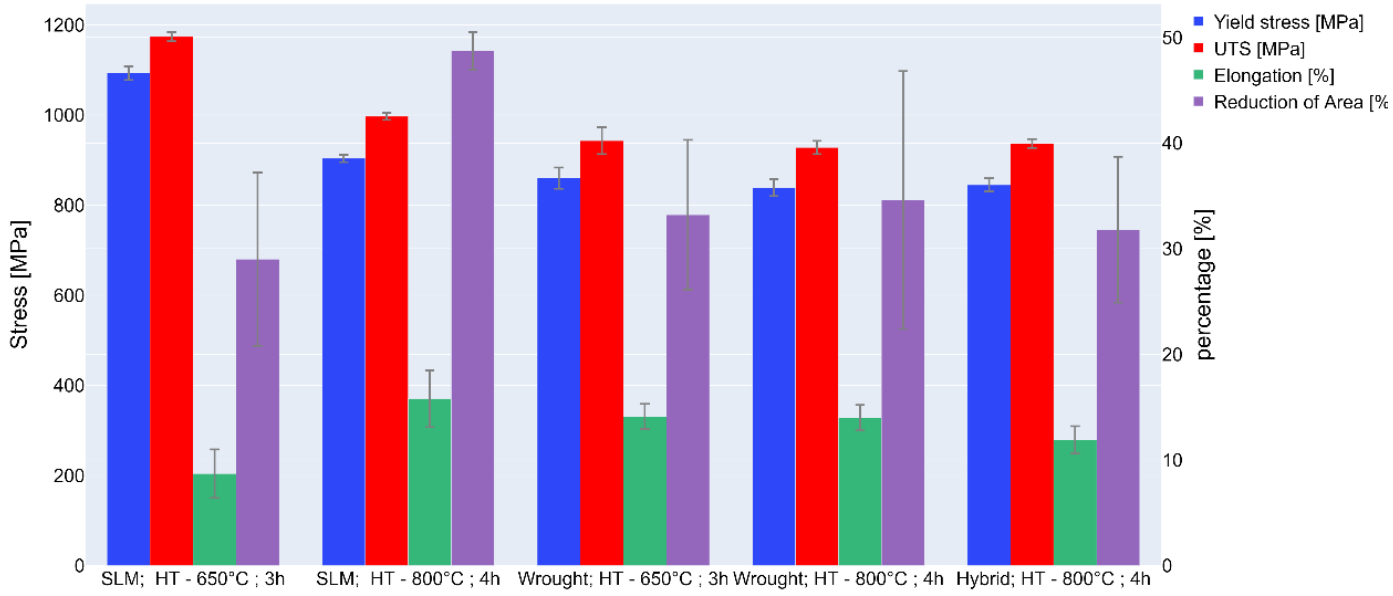

Figure 6: A comparison of the uniaxial tensile test results between the different tested groups.

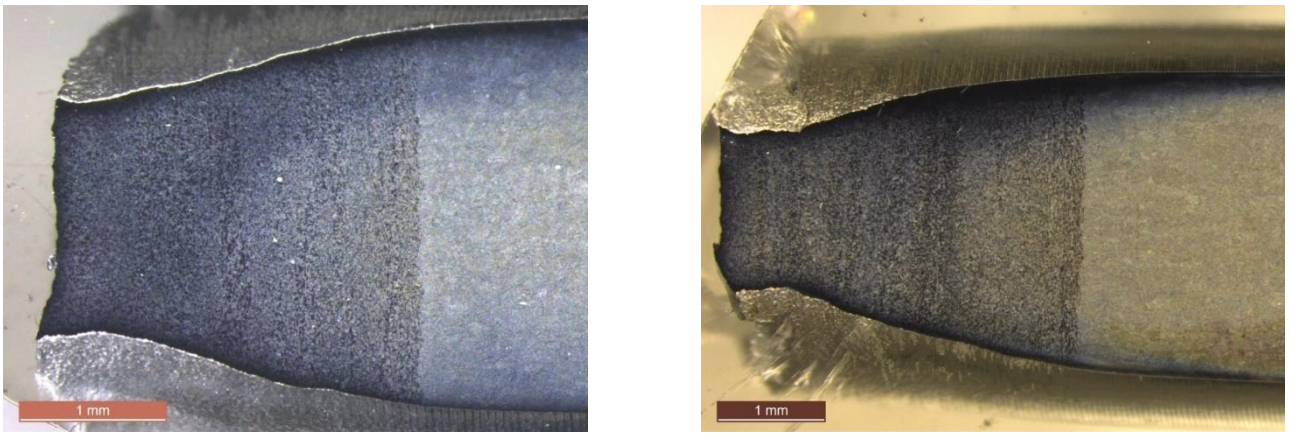

Figure 7: Typical tensile hybrid specimens post-failure. The specimens were ground, polished, and etched to aid in visualizing the location of the interface. Note that necking and failure have occurred in the wrought side and more than 1mm away from the wrought/AM interface.

To further investigate the mechanical behavior under tension of the hybrid specimen, and specifically, the strain partitioning between the two materials composing the hybrid tensile specimen, the strain evolution strain along the hybrid specimen's gauge section is given in Figure 8. From figure 8 it is clear that while the wrought side of the specimens carries the majority of deformation, its AM counterpart has only yielded to a limited extent. Both SEM and computed x-ray tomography of the failed hybrid specimen did not reveal an increased level of porosity at the AM side of the specimen, inline with the strain measurements and the relatively large distance between the necking region and AM/wrought interface.

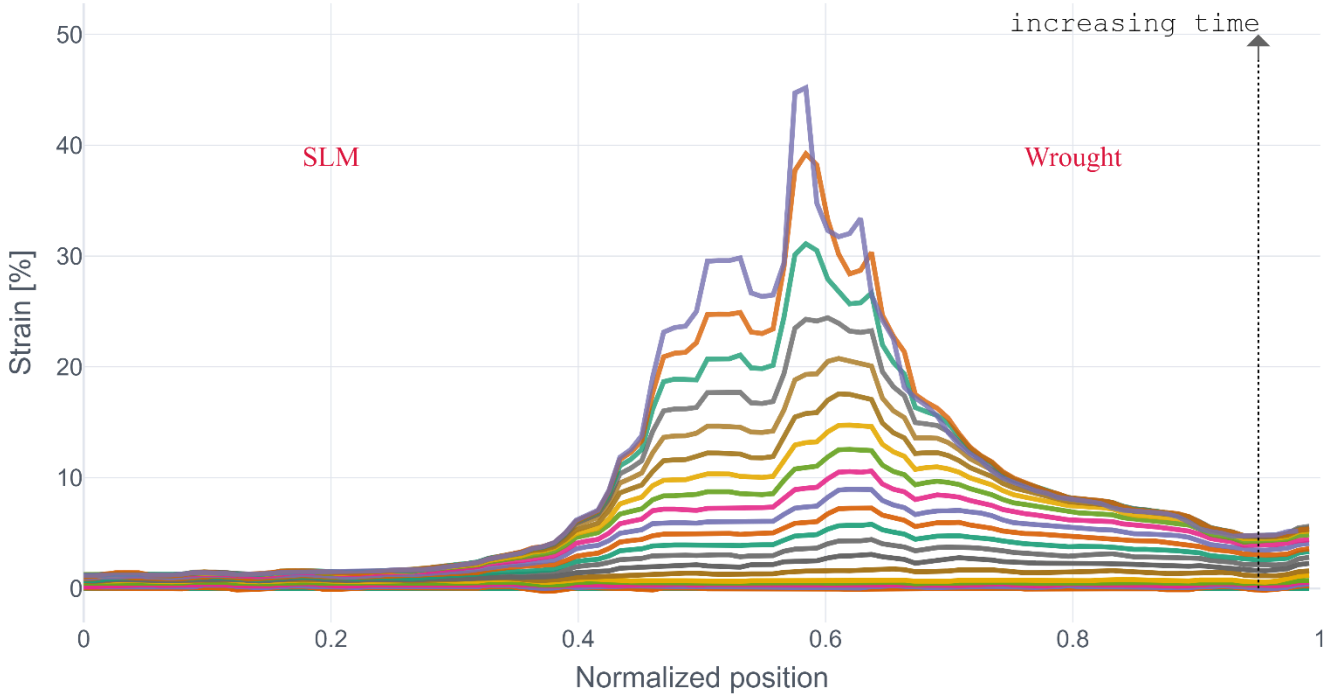

Figure 8: DIC measurements, showing the strain evolution along a path aligned with the tensile direction over time. Note, that since the path over which the strain was extracted is chosen inside the GOM software, the precise allocation of the interface was hard to achieve. Thus, the normalized position does not mean that the interface lies at 0.5 but rather somewhere in its vicinity.

3.3 Fracture toughness

The fracture toughness samples were prepared and tested in accordance with the International Standard Test Method for Linear-Elastic Plane-Strain Fracture Toughness KIC of Metallic Materials ASTM E399-17. The choice of sample geometry (Figure 2b) was somewhat limited due to the geometric restrictions imposed by the wrought plate dimensions and CT25 specimens were extracted from the In-plane direction of the plate. Similar to the testing plan in Section 3.2, the wrought and AM materials were tested for both heat treatments, as to set a baseline for the measurements of the hybrid material. The test groups and number of specimens within each are summarized in Table 3.

Table 3: Fracture toughness results of wrought material, AM and hybrid samples

Sample description	Number of samples	K_{IC} [MPa $\sqrt{m}$]		Pmax [KN]
Wrought; HT - 650°C ; 3h	4	77.5	±13.3	15.39
Wrought; HT - 800°C ; 4h	4	69.8	±14.1	13.61
SLM; HT - 650°C ; 3h - along Z	5	45.7	±4.6	13.28
SLM; HT - 800°C ; 4h - along Z	4	61.8	±13.6	12.66
Hybrid; HT - 800°C ; 4h - along Z	4	89.4	±13.6	18.41
Hybrid; HT - 800°C ; 4h - Top	4	85.5	±3.6	17.92
Hybrid; HT - 800°C ; 4h - Flat	4	83.5	±2.3	17.95

While the tensile properties of the wrought material were found to be only weakly sensitive to the choice of heat treatment, the fracture toughness was observed to vary by close to 10% between the two heat treatments, making the 650°C/3h favorable. In the AM, the relative difference between the two test conditions yields a toughening of roughly 26%, in accordance with the improved ductility observed for the tensile tests. It is worth noting that the SLM material's response to the studied heat treatments is exactly opposite to that of the wrought material with 800°C/4h being the preferred heat treatment.

Due to the higher sensitivity of the AM material to the selected heat treatment and the opposite effect the heat treatments have on the measured fracture toughness, the large difference in K_{IC} between the AM and wrought materials resulting from the 650°C/3h treatment (~40%) is considerably reduced for the 800°C/4h (~11%). In order to test the hybrid material at conditions for which its two constituents have similar KIC values, as well to remain consistent with the test program of section 3.2, all of the hybrid fracture specimens were treated at 800°C/4h.

The results of the fracture toughness experiments are summarized in Figure 9. The three groups of hybrid materials, regardless of their orientation, have demonstrated higher fracture toughness (and maximum load) than the specimens belonging to either the AM or wrought category. Here we note, that while we are aware to the fact that the ASTM formula used to calculate K_{IC} from the measured loads during the experiment is invalid for a bi-material[39,40], The relative differences between the two materials hardening curve are not very big and thus we consider the classical equation to be a decent approximation. Nonetheless, even if ignoring the actual K_{IC} values, the maximum loads leading to crack propagation are substantially higher for the hybrid specimens.

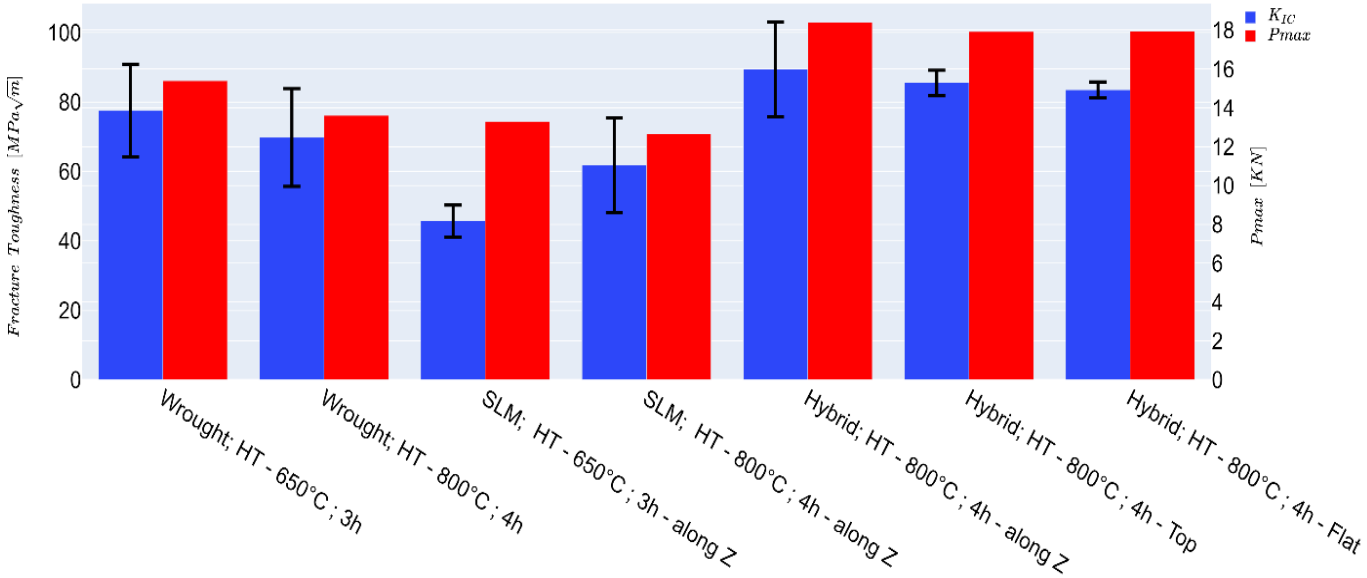

Figure 9: A comparison of the fracture test results between the different tested groups.

.

In all of the flat hybrid fracture tests, the fatigue pre-crack was observed to grow in a non-uniform manner (Figure 10), propagating faster in the wrought side during the fatigue pre-cracking process. Nonetheless, No evidence for abrupt crack growth on one of the sides (i.e. AM/Wrought) was observed and it appears that the fatigue crack, albeit being non-uniform has grown in a continuous manner. To estimate the toughenss in the presence of non uniform pre-crack fronts, , the post-mortem measured fatigue crack length, required for the KIC calculation was determined by averaging the actual crack length taken from five evenly distributed measurement along the crack front. Contradictory to the report of Zhang et al. [11] where the crack growth in a wire arc additive manufactured Ti-6Al-4V hybrid material was observed to grow into the substrate material, here the crack appeared to adhere to the geometrical symmetry plane of the specimen with some

undulations between the AM and wrought parts. In [11], the crack path selection was rationalized with respect to the residuals strains which were mapped along the specimen. Also, a clear HAZ was reported near the WAAM-wrought interface. It is plausible that the minor (if any) residual stresses in our hybrid material, in conjunction with the absence of a HAZ are the main cause for the discrepancy between the observations drawn here and in [11].

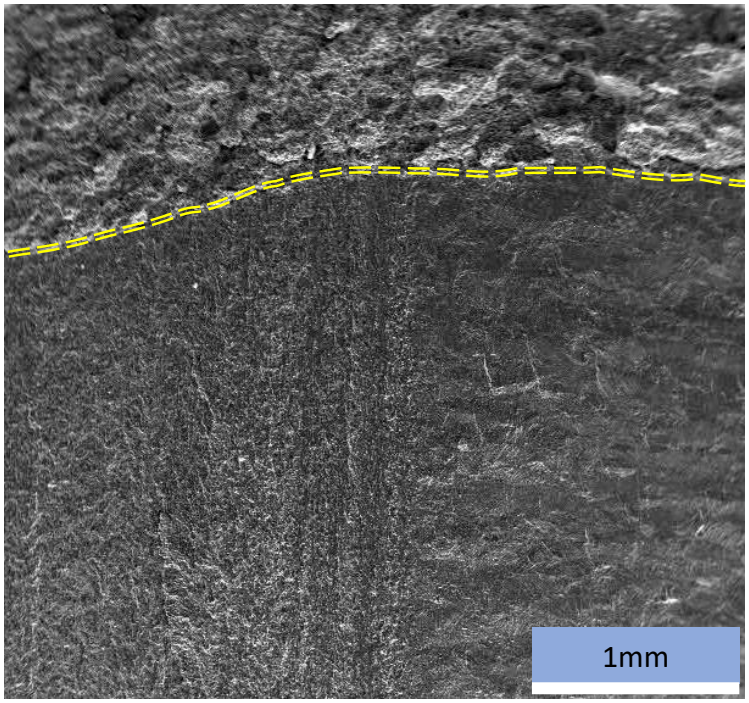

Figure 10: A comparison of the fracture test results between the different tested groups.

4. Summary and Conclusions

The uniaxial tensile ductility as well as the plane strain fracture toughness of a hybrid AM-wrought Ti-6Al-4V alloy were investigated and compared with the AM and wrought materials serving as a baseline. The main findings of this work are:

- The hybrid specimens did not exhibit any type of defects in the vicinity of the interface. Furthermore, the micro-hardness values were recovered to those expected from the individual materials within 100μm for the case of the wrought alloy and 200μm for the AM one.
- No HAZ was observed in the hybrid material, presumably due to the diminishing heating cycles associate with the printing process and their relatively short duration (per cycle).
- The two heat treatments considered in this work, were found to have negligible effect on the tensile properties of the wrought material while drastically improving the tensile ductility of the AM material.
- Hybrid AM-wrought tensile specimens were shown to localize the majority of deformation in the wrought material with little to no plasticity observed in its AM counterpart.
- The fracture toughness of AM and wrought samples was observed to react in an opposing trend when subjected to the same heat treatments. At this stage this is merely an observation, but one which merits further investigation.
- It was found that the fracture toughness of the hybrid material is superior to that of either the AM or the wrought alloy. The unique crack tip constrains emerging at a bi-material interface are not sufficient to explain this observation as this observation prevailed also for the “Flat” and “Top” specimens at which crack propagation was not along the interface.

To summarize, we have shown that *Hybrid manufacturing of load-bearing, damage-critical, Ti-6Al-4V components, is indeed a viable option*. While their fatigue tolerance is yet to be investigated, both the tensile and fracture toughness results are extremely promising. During this investigation, several peculiarities, which we did not anticipate a-priori have been observed. Despite the vast body of knowledge gathered in recent years regarding the differences between wrought and AM Ti-6Al-4V, we are not aware of any publication in which the opposite trends we identified were previously emphasized and explored.

5. Acknowledgements

The authors would like to acknowledge the assistance of the technical staff in the Israel Institute of Metallurgy at the Technion – Israel Institute of Technology and the Materials Processing group at Rafael Metal Technology Center for their technical assistance along this work. S.O would like to gratefully acknowledge the financial support provided by the Pazy foundation through the young researchers award Grant #1176.

6. References

[1] G. Welsch, R. Boyer, E.W. Collings, Materials properties handbook: titanium alloys, ASM international, 1993.

[2] C. Leyens, M. Peters, Titanium and titanium alloys: fundamentals and applications, John Wiley & Sons, 2003.

[3] G. Lütjering, J.C. Williams, Titanium, Springer Science & Business Media, 2007.

[4] P. Singh, H. Pungotra, N.S. Kalsi, On the characteristics of titanium alloys for the aircraft applications, Mater. Today Proc. 4 (2017) 8971–8982.

[5] A. Leon, G.K. Levy, T. Ron, A. Shirizly, E. Aghion, The effect of hot isostatic pressure on the corrosion performance of Ti-6Al-4V produced by an electron-beam melting additive manufacturing process, Addit. Manuf. (2020) 101039.

[6] A. Leon, G.K. Levy, T. Ron, A. Shirizly, E. Aghion, The effect of strain rate on stress corrosion performance of Ti6Al4V alloy produced by additive manufacturing process, J. Mater. Res. Technol. (2020).

[7] B.P. Conner, G.P. Manogharan, A.N. Martof, L.M. Rodomsky, C.M. Rodomsky, D.C. Jordan, J.W. Limperos, Making sense of 3-D printing: Creating a map of additive manufacturing products and services, Addit. Manuf. 1 (2014) 64–76.

[8] B. Dutta, F.H.S. Froes, The additive manufacturing (AM) of titanium alloys, in: Titan. Powder Metall., Elsevier, 2015: pp. 447–468.

[9] S. Leuders, M. Thöne, A. Riemer, T. Niendorf, T. Tröster, H.A. a Richard, H.J. Maier, On the mechanical behaviour of titanium alloy TiAl6V4 manufactured by selective laser melting: Fatigue resistance and crack growth performance, Int. J. Fatigue. 48 (2013) 300–307.

[10] P. Edwards, M. Ramulu, Effect of build direction on the fracture toughness and fatigue crack growth in selective laser melted Ti-6Al-4 V, Fatigue Fract. Eng. Mater. Struct. 38 (2015) 1228–1236.

[11] J. Zhang, X. Zhang, X. Wang, J. Ding, Y. Traoré, S. Paddea, S. Williams, Crack path selection at the

interface of wrought and wire+ arc additive manufactured Ti--6Al--4V, Mater. Des. 104 (2016) 365–375.

[12] P. Kumar, U. Ramamurty, Microstructural optimization through heat treatment for enhancing the fracture toughness and fatigue crack growth resistance of selective laser melted Ti6Al4V alloy, Acta Mater. 169 (2019) 45–59.

[13] R. Fadida, A. Shirizly, D. Rittel, Dynamic tensile response of additively manufactured Ti6Al4V with embedded spherical pores, J. Appl. Mech. 85 (2018).

[14] A.H. Chern, P. Nandwana, T. Yuan, M.M. Kirka, R.R. Dehoff, P.K. Liaw, C.E. Duty, A review on the fatigue behavior of Ti-6Al-4V fabricated by electron beam melting additive manufacturing, Int. J. Fatigue. 119 (2019) 173–184. doi:10.1016/j.ijfatigue.2018.09.022.

[15] L. Novotný, M. Béreš, H.F.G. de Abreu, J. Zajac, W. Bleck, Thermal analysis and phase transformation behaviour during additive manufacturing of Ti–6Al–4V alloy, Mater. Sci. Technol. (United Kingdom). 35 (2019) 846–855. doi:10.1080/02670836.2019.1593669.

[16] C. Chen, Y. Xie, X. Yan, S. Yin, H. Fukanuma, R. Huang, R. Zhao, J. Wang, Z. Ren, M. Liu, H. Liao, Effect of hot isostatic pressing (HIP) on microstructure and mechanical properties of Ti6Al4V alloy fabricated by cold spray additive manufacturing, Addit. Manuf. 27 (2019) 595–605. doi:10.1016/j.addma.2019.03.028.

[17] S. Liu, Y.C. Shin, Additive manufacturing of Ti6Al4V alloy: A review, Mater. Des. 164 (2019) 107552. doi:10.1016/j.matdes.2018.107552.

[18] M. Merklein, D. Junker, A. Schaub, F. Neubauer, Hybrid additive manufacturing technologies - An analysis regarding potentials and applications, Phys. Procedia. 83 (2016) 549–559. doi:10.1016/j.phpro.2016.08.057.

[19] B. Nau, A. Roderburg, F. Klocke, Ramp-up of hybrid manufacturing technologies, CIRP J. Manuf. Sci. Technol. 4 (2011) 313–316. doi:10.1016/j.cirpj.2011.04.003.

[20] L. Li, Repair of directionally solidified superalloy GTD-111 by laser-engineered net shaping, J. Mater. Sci. 41 (2006) 7886–7893. doi:10.1007/s10853-006-0948-0.

[21] J. Song, Q. Deng, C. Chen, D. Hu, Y. Li, Rebuilding of metal components with laser cladding forming, Appl. Surf. Sci. 252 (2006) 7934–7940. doi:10.1016/j.apsusc.2005.10.025.

[22] L. Sexton, S. Lavin, G. Byrne, A. Kennedy, Laser cladding of aerospace materials, J. Mater. Process. Technol. 122 (2002) 63–68. doi:10.1016/S0924-0136(01)01121-9.

[23] D.D. Gill, J.E. Smugeresky, M.F. Harris, C. V Robino, M.L. Griffith, On the Interface Between LENS®Deposited Stainless Steel 304L Repair Geometry and Cast or Machined Components, Sandia Rep. (2004).

[24] H. Kim, W. Cong, H.-C. Zhang, Z. Liu, Laser engineered net shaping of nickel-based superalloy Inconel 718 powders onto AISI 4140 alloy steel substrates: Interface bond and fracture failure mechanism, Materials (Basel). 10 (2017) 341.

[25] C. Tan, K. Zhou, W. Ma, L. Min, Interfacial characteristic and mechanical performance of maraging steel-copper functional bimetal produced by selective laser melting based hybrid manufacture, Mater. Des. 155 (2018) 77–85. doi:10.1016/j.matdes.2018.05.064.

[26] E. Cyr, H. Asgari, S. Shamsdini, M. Purdy, K. Hosseinkhani, M. Mohammadi, Fracture behaviour of additively manufactured MS1-H13 hybrid hard steels, Mater. Lett. 212 (2018) 174–177. doi:10.1016/j.matlet.2017.10.097.

[27] H. Azizi, R. Ghiaasiaan, R. Prager, M.H. Ghoncheh, K.A. Samk, A. Lausic, W. Byleveld, A.B. Phillion, Metallurgical and mechanical assessment of hybrid additively-manufactured maraging tool

steels via selective laser melting, Addit. Manuf. 27 (2019) 389–397. doi:10.1016/j.addma.2019.03.025.

[28] S. Shakerin, A. Hadadzadeh, B.S. Amirkhiz, S. Shamsdini, J. Li, M. Mohammadi, Additive manufacturing of maraging steel-H13 bimetals using laser powder bed fusion technique, Addit. Manuf. 29 (2019) 100797. doi:10.1016/j.addma.2019.100797.

[29] A. Schaub, V. Juechter, R.F. Singer, M. Merklein, Characterization of hybrid components consisting of SEBM additive structures and sheet metal of alloy Ti-6Al-4V, in: Key Eng. Mater., 2014: pp. 609–614.

[30] B. Ahuja, A. Schaub, M. Karg, R. Schmidt, M. Merklein, M. Schmidt, high power laser beam melting of Ti-6Al-4V on formed sheet metal to achieve hybrid structures, in: Laser 3D Manuf. II, 2015: p. 93530X.

[31] F. Huber, T. Papke, M. Kerkien, F. Tost, G. Geyer, M. Merklein, M. Schmidt, Customized exposure strategies for manufacturing hybrid parts by combining laser beam melting and sheet metal forming, J. Laser Appl. 31 (2019) 22318.

[32] L. Butzhammer, P. Dubjella, F. Huber, A. Schaub, M. Aumüller, O. Petrunenko, M. Merklein, M. Schmidt, Experimental investigation of a process chain combining sheet metal bending and laser beam melting of Ti-6Al-4V, Lasers in Manufactuing (LiM). (2017).

[33] X. Shi, S. Ma, C. Liu, Q. Wu, J. Lu, Y. Liu, W. Shi, Selective laser melting-wire arc additive manufacturing hybrid fabrication of Ti-6Al-4V alloy: Microstructure and mechanical properties, Mater. Sci. Eng. A. 684 (2017) 196–204.

[34] J.J. Lewandowski, M. Seifi, Metal Additive Manufacturing: A Review of Mechanical Properties, Annu. Rev. Mater. Res. 46 (2016) 151–186. doi:10.1146/annurev-matsci-070115-032024.

[35] Y. Kok, X.P. Tan, P. Wang, M.L.S. Nai, N.H. Loh, E. Liu, S.B. Tor, Anisotropy and heterogeneity of microstructure and mechanical properties in metal additive manufacturing: A critical review, Mater. Des. 139 (2018) 565–586. doi:10.1016/j.matdes.2017.11.021.

[36] Y. Zhu, J. Li, X. Tian, H. Wang, D. Liu, Microstructure and mechanical properties of hybrid fabricated Ti-6.5Al-3.5Mo-1.5Zr-0.3Si titanium alloy by laser additive manufacturing, Mater. Sci. Eng. A. 607 (2014) 427–434. doi:10.1016/j.msea.2014.04.019.

[37] J. Zhang, X. Wang, S. Paddea, X. Zhang, Fatigue crack propagation behaviour in wire+arc additive manufactured Ti-6Al-4V: Effects of microstructure and residual stress, Mater. Des. 90 (2016) 551–561. doi:10.1016/j.matdes.2015.10.141.

[38] B. Tavlovich, A. Shirizly, R. Katz, EBW and LBW of additive manufactured Ti6Al4V products, Weld J. 97 (2018) 179S--190S.

[39] H. Lee, Y. Kim, Interfacial crack-tip constraints and J -integral for bi-materials with plastic hardening mismatch, Int. J. Fract. (2007) 231–243. doi:10.1007/s10704-006-9025-6.

[40] C.F. Shih, Cracks on bimaterial interfaces : elasticity and plasticity aspects, Mater. Sci. Eng. A. 143 (1991) 77–90.